Control and Operation of A New 8/6-Pole Split-Winding Doubly Salient Permanent Magnet Motor Drive

Cheng Ming[1], K.T. Chau[2] and C.C. Chan[2]

1 Department of Electrical Engineering, Southeast University, Nanjing 210096, China
2 Department of Electrical and Electronic Engineering, The University of Hong Kong, Hong Kong, China

Abstract—**This paper proposes a new 8/6-pole split-winding doubly salient permanent magnet (DSPM) motor drive. The analysis, control, implementation and experiments of the motor drive are presented. The magnetic field analysis is carried out using finite element method. The split-winding topology is proposed to extend the constant power operation range. The control strategy for the DSPM motor drive is developed. Two operation modes, namely 4-phase and 2-phase operation modes, are proposed for the 8/6-pole DSPM motor drive. In 4-phase operation mode, a half-bridge power converter but without split capacitors is used to reduce the number of power devices and to eliminate the problem of voltage unbalance in the capacitors. The drive system is implemented and tested. The experimental results show that the developed control scheme can operate the DSPM motor properly, and the DSPM motor drive offers high efficiency over wide power range and good dynamic performance. Furthermore, the 2-phase operation mode of the 8/6-pole DSPM motor offers the potentiality of eliminating the torque ripple of the motor drive.**

I. INTRODUCTION

It has been a long-standing goal to develop an advanced motor drive that combines the advantages of the DC motor drive of good speed controllability and the AC motor drive of high reliability, robustness, and maintenance free for industry and electric vehicle applications. In the past decades, many advanced motor drives with improved efficiency using permanent magnets in the motor have been developed [1], [2]. One of those high efficiency advanced motors is the doubly salient permanent magnet (DSPM) motor [3]. The recent literature has shown that the DSPM motor is of high efficiency, high power density and simple structure [3]-[7].

Recently, a new 4-phase, 8/6-pole DSPM motor has been proposed and its definite advantages over a 6/4-pole one, namely higher power density, wider speed range, less torque ripple, and lower current magnitude, have been revealed [4]. However, similar to most of the PM brushless motors, the constant power operation range of the DSPM motor is very limited due to the fact that the field control capability of PM excitation is more difficult to achieve than that of wound field excitation. The purpose of this article is to propose a new topology to extend the constant power operation range of the DSPM motor, namely split-winding configuration. The

analysis, control, implementation and performance of the proposed split-winding DSPM motor drive are presented. To operate the DSPM motor in bi-directional current, a 4-phase half-bridge power converter but without split capacitors is used so as to reduce the number of devices, and to eliminate the problem of voltage unbalance in the split capacitors. The control strategy for the proposed DSPM motor drive is explored and implemented based on a 16-bit high-speed microcomputer. The experimental results of the prototype machine not only verify the theoretical analysis, but also show that the developed DSPM motor drive offers high efficiency over wide output power range and good dynamic performance. The split-winding topology can effectively extend the constant power operation range of the DSPM motor. Furthermore, according to the unique feature of the 8/6-pole DSPM motor, a new two-phase operation mode is proposed, which offers the potentiality of eliminating the torque ripple of the motor drive.

II. MOTOR STRUCTURE AND MAGNETIC FIELD ANALYSIS

Fig. 1 shows the cross section of the newly proposed DSPM motor. It is a 4-phase, 8/6-pole DSPM motor and essentially adopts the same structure as a switched reluctance (SR) motor, but with permanent magnets placed in the stator. There is no permanent magnets or windings in the rotor. Obviously, the machine is of simple structure and free of maintenance, and is capable of working at high speed. The corresponding PMs are located in stator and thus can be easily cooled, hence eliminating the problem of irreversible demagnetization and mechanical instability. In addition, since the stator windings are concentrated, the overhanging part of the coil is short, resulting in the saving of copper as well as the reduction of copper loss.
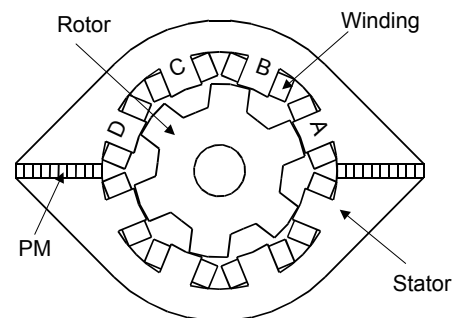

Fig. 1. Cross-section of 8/6-pole DSPM motor.

Under assumptions that the fringing offset is negligible, and the permeability of the core is infinite, a linear variation of PM flux linkage is produced in each of stator windings at no-load. The corresponding theoretical waveforms of PM flux and phase current are shown in Fig. 2. When PM flux linkage increases with rotor position angle, a positive phase current is applied to the winding, resulting in a positive torque. When PM flux linkage decreases, a negative current is applied to the winding, also resulting in a positive torque. Thus the two possible torque-producing zones are all utilized.
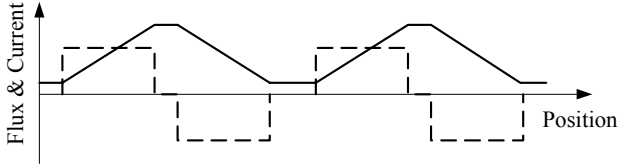

Fig. 2. Theoretical flux (solid) and current (dashed) waveforms.

The magnetic field of the motor has been analyzed by finite element method [5]. Fig. 3 gives the distributions of the PM field at no-load and the armature field at the phase current of 2A. It can be seen from Fig. 3(a) that most of the flux produced by PMs loops through the air gap and rotor. Additionally there is a little flux passing through the surrounding space outside the circumference of the motor, which is the outer leakage flux peculiar to the DSPM motor. Fig. 3(b) shows that most of the armature flux loops through adjacent stator poles and only a little portion passes through the PMs. Therefore, the DSPM motor is less sensitive to the demagnetizing effect of the armature flux than traditional PM machines. From the finite element analysis, the static characteristics, namely PM flux linkage, back EMF and phase inductance, can readily be deduced [5].

III. SPLIT-WINDING TOPOLOGY

According to the operation principle of the DSPM motor, the maximum speed of a DSPM motor for given supply voltage can be deduced as [4], [7]:

$$\omega_{r\max} = \frac{U}{kwB_g} \tag{1}$$

where U is the voltage applied to phase winding, k a constant factor governed by machine dimensions, w the turn number of winding per phase in series, B_g the flux density in the air gap. Equation (1) indicates that the speed limit can be extended by reducing the number of winding turns per phase. This principle of extending operation range is suitable to all PM motors in theory, but not practical for those normal PM motors, such as PM synchronous motors, because they adopt distributed windings and the corresponding change of winding turns is difficult. However, the DSPM motor with concentrated winding can allow changing the number of winding turns by employing split-windings [7], [8]. Fig. 4 shows the

schematic connection of the proposed split-windings. When the switch K_1 is on, the whole windings are functional, whereas the switch K_2 can be turned on so that the winding turns per phase are reduced to 50%. Fig. 5 gives the simulated steady-state torque characteristics under different winding turns, showing that the constant power operation range of the motor is much extended by reducing the winding turns from 100% to 50%.
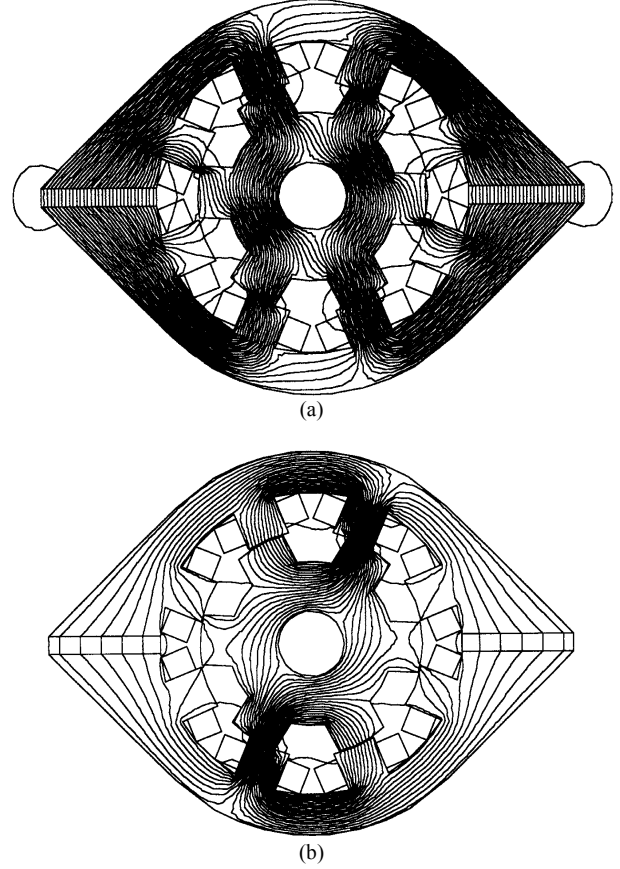

(a)

(b)

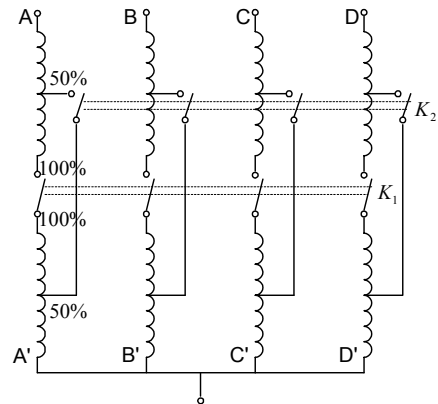Fig. 3. Magnetic field distribution. (a) PM field; (b) Armature field.
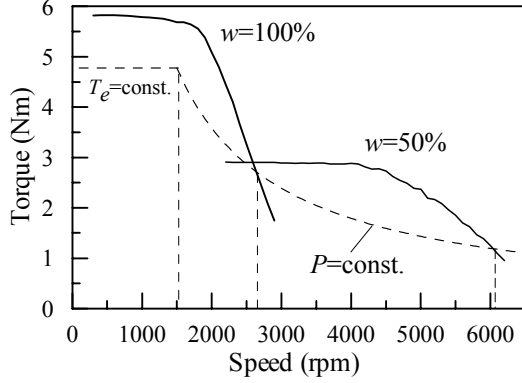

Fig. 4. Schematic connection of split-windings.

127

Fig.5. Simulated torque characteristics under different winding turns.

IV. CONTROL STRATEGY

The speed of the DSPM motor drive is controlled by a digital PI controller whose output is the torque reference T_e^*. The discrete equation for digital PI controller can be obtained as [9]:

$$T(k) = K_P e(k) + K_I \sum_{j=0}^{k} e(j) = T_P(k) + T_I(k) \qquad (2)$$

where e is the speed offset, K_P and K_I are the proportional and integral gains, respectively. To reduce speed oscillation, a small dead zone of speed is deliberately introduced into the controller. To speed up the dynamic response, the bang-bang control is combined with the PI control. When the absolute value of the speed offset is larger than a given value ε, the bang-bang control is adopted. Otherwise, PI control is performed:

$$\begin{cases} e(k) > \varepsilon \cdots \text{bang\_bang control} \\ e(k) \le \varepsilon \cdots \text{PI control} \end{cases} \qquad (3)$$

In bang-bang control, if the speed error is positive and the speed is increasing, the output of the controller is directly set to be the maximum. Otherwise, it is set to be zero.

In DSPM motor, four angles, namely θ_{on}^+, θ_{off}^+, θ_{on}^- and θ_{off}^-, as well as current reference are possible control variables to shape the phase current, which can give a very flexible control schemes. Hence, the torque of the motor can be controlled by the current chopping control (CCC) and angle position control (APC), respectively for constant torque operation at speeds below the base speed and constant power operation at speeds above the base speed. In the low speed CCC mode, the four angles are fixed and the torque is controlled by current reference I^*. According to the principle of the DSPM motor, the electromagnetic torque per phase can be expressed as [4]:

$$T_e = i_s \frac{d\psi_{pm}}{d\theta} + \frac{1}{2} i_s^2 \frac{dL}{d\theta} = T_{pm} + T_r \qquad (4)$$

where ψ_{pm} is the PM-induced flux linkage, L phase inductance, θ rotor position angle, i_s phase current, T_r reluctance torque component, and T_{pm} PM torque component. Since the current waveforms in the positive and negative strokes are symmetrical in CCC mode, the average value of reluctance torque component is zero. Thus, the average torque of the motor is governed by the PM torque component only, which is given by:

$$T_{av} = \frac{2m}{\theta_{cr}} \int_{\theta_{on}^+}^{\theta_{off}^+} \left(I \frac{d\psi_{pm}}{d\theta} \right) d\theta \approx \frac{2m}{\theta_{cr}} I(\psi_{pm2} - \psi_{pm1}) \qquad (5)$$

where I is the magnitude of the rectangular waveform current, m phase number, θ_{cr} the rotor pole pitch angle, ψ_{pm1} and ψ_{pm2} are the PM flux linkages corresponding to θ_{on}^+ and θ_{off}^+, respectively. It is seen that the average torque is proportional to the current I. Hence, once the torque reference T_e^* is obtained by using PI regulation, the current reference I^* can readily be specified using (5).

In high speed APC mode, the torque is controlled by conduction angle θ_w, which is given by:

$$\theta_w = \theta_{off}^+ - \theta_{on}^+ = \theta_{off}^- - \theta_{on}^- \qquad (6)$$

Fig. 6 illustrates the measured current waveform of the motor with light load at the APC mode.
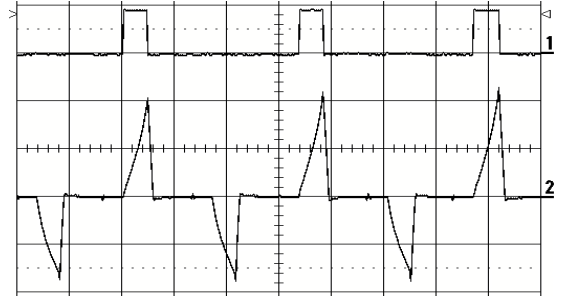

Fig. 6. Measured phase current (lower trace) and the positive stroke firing signal (upper trace) waveforms at APC mode with light load.

Fig. 7 shows the control block diagram of the DSPM motor drive. The core of the control system is an Intel 80C196KD 16-bit high-speed microcomputer. It receives position signals from the rotor position sensor and calculates the speed and firing angles. The microcomputer also produces current references to the IGBTs of the converter. The phase current is measured by the LEM module and is fed back to a hysteresis controller for current chopping control. To simplify the comparison of the measured current with the current reference, an absolute value amplifier is adopted to convert the AC current to DC current for each phase. Fig. 8 illustrates the circuitry of the absolute value amplifier and its input and output signal waveforms at 20 kHz, showing a very small distortion.
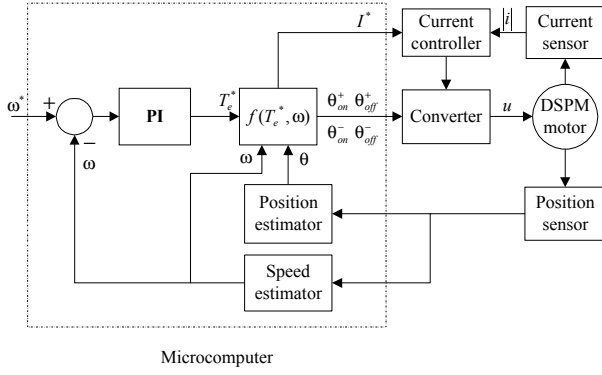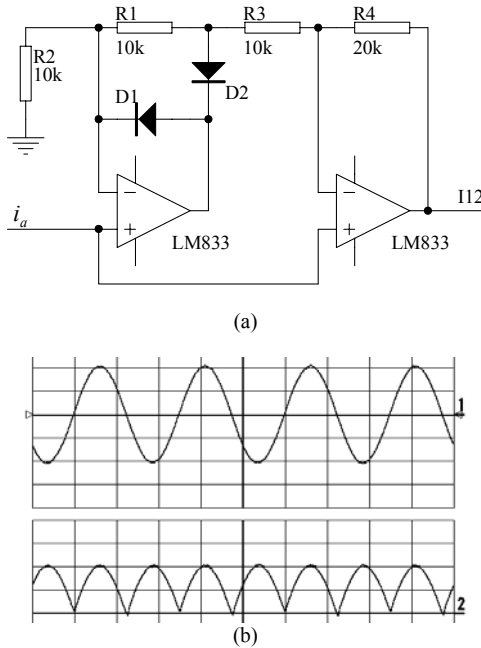
Fig. 7. Control block diagram.

(a)

(b)

Fig. 8. Absolute value amplifier. (a) Circuitry; (b) Input (upper trace) and output (lower trace) waveforms at 20 kHz.

In accordance with the operation principle of the DSPM motor, the phase winding should be turned on or off at the specific rotor positions. Hence the rotor position information is indispensable for the proper operation of the DSPM motor. For the motor drive system developed in this paper, positions are measured by a simple position sensor (PS). As shown in Fig. 9, this PS consists of a slotted disc connected to the rotor shaft and two opto-couplers mounted to the stator housing. The two opto-couplers are nominally located 45° apart from each other along the circumference of the disc. The output waveforms of the sensor are shown in Fig. 10. The sensor generates a signal edge for every 15° of mechanical rotation. The transitions of these outputs determine specific angles. At each edge, the speed is calculated by:

$$\hat{n} = \frac{60\Delta r}{\Delta t} = \frac{f_{clk}}{0.4N} \qquad (7)$$

where $\hat{n}$ is the speed in rpm, Δr the distance between edges in revolution, Δt the time between edges, N the number of clock counts between edges, and f_{clk} the clock frequency.

For the proposed 4-phase 8/6-pole DSPM motor, the control logic can be obtained as given in Table I according to the relationship between the PM fluxes and position signals in Fig. 10.
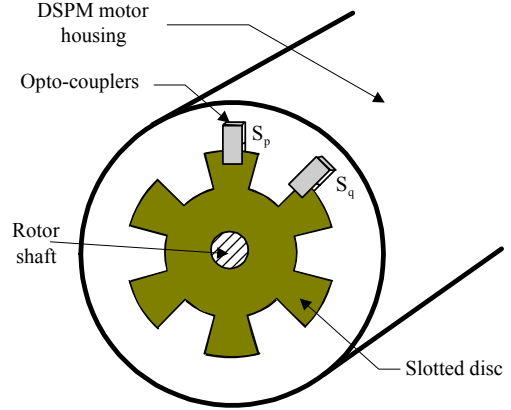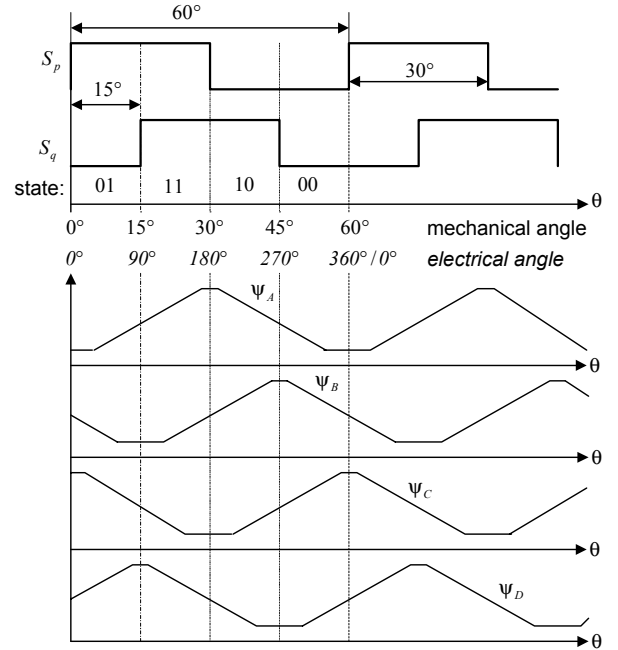

Fig. 9. Position sensor.

Fig. 10. Position signals and PM flux linkages.

V. OPERATION MODES OF 8/6-POLE DSPM MOTOR DRIVE

To supply the DSPM motor, a bipolar converter is preferred so as to bring the merit of the DSPM motor into full play. To control the phase currents individually, there are basically two converter topologies possible for bi-directional operation of the DSPM motor, namely the full-bridge converter, and the half-bridge converter with split capacitors.

129

The later topology is usually selected for the DSPM drive system, because it minimizes the use of power devices, as shown in Fig. 11.

TABLE I
CONTROL LOGIC OF DSPM MOTOR DRIVE

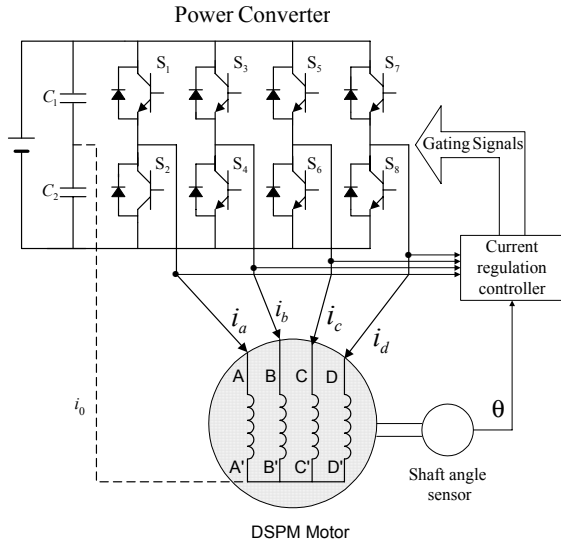| Signal states: $S_q S_p$		01	11	10	00
Phase A	S_1	1	1	0	0
	S_2	0	0	1	1
Phase B	S_3	0	1	1	0
	S_4	1	0	0	1
Phase C	S_5	0	0	1	1
	S_6	1	1	0	0
Phase D	S_7	1	0	0	1
	S_8	0	1	1	0

Power Converter

Fig. 11. Schematic diagram of the DSPM motor drive.

A. Four Phase Operation

For 3-phase 6/4-pole DSPM motors [3], [10], the connection between the center-point of the split capacitors and the neutral of motor windings, as shown by the dotted line in Fig. 11, is usually necessary to accommodate the additional current during the commutation period. However, voltage asymmetry between the two split capacitors often occurs because the phase currents are asymmetrical in the DSPM motor [4]. As a result, different voltages are applied to the upper and lower legs, which reduces the dynamic behavior of the motor drive, increases the torque ripple, and even damages the capacitors and the control system. Therefore, some auxiliary hardware and software are necessary to keep the voltage at the center-point of the capacitors almost constant [10], [11], which makes the control system more complicated.

For the proposed 4-phase 8/6-pole DSPM motor, however, it can be found from the control logic given in Table I that at any time instant the power switches in upper and lower legs

of the converter are conducting in pairs (phase A pairs up with phase C, and phase B pairs up with phase D). Hence it arises the possibility of removing the connection between the center-point of the split capacitors and the neutral of the motor windings without significant influence on the behavior of the motor drive provided $\theta_{on}^- = \theta_{on}^+ + \frac{1}{2}\theta_{cr}$ and $\theta_{off}^- = \theta_{off}^+ + \frac{1}{2}\theta_{cr}$. As a consequence, the problem of voltage unbalance in the split capacitors is eliminated and the hardware and software of the control system are thus simplified. Moreover, because the positive half cycle and negative half cycle of the phase current are forced to be almost symmetrical, the average value of the reluctance torque become near zero even at high speed.

B. Two phase operation

Further inspecting the characteristics and the control logic of the 8/6-pole DSPM motor drive reveals that there is a possibility of the DSPM motor working as two-phase motor drive. Reversely connecting the winding A with C and winding B with D, respectively, in series, as shown in Fig. 12, we can construct a two-phase DSPM motor drive. It can be supplied by a two-phase full-bridge power converter or a half-bridge power converter with split capacitors. In the former case, the supply DC bus voltage and the number of power switches are the same as those in four phase operation mode with half-bridge converter in Fig. 11, but the voltage rating of power switches is halved and in turn the cost and loss of power switches may be reduced.
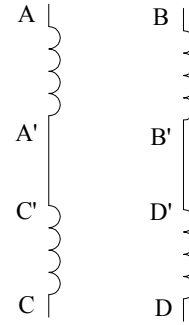

Fig. 12. Winding connection of two-phase operation mode of 8/6-pole DSPM motor.

What is more important is that the two-phase operation mode offers the potentiality of eliminating the torque ripple of the motor drive. The self-inductance of each phase in two-phase mode should be equal to the summation of Phases A and C or Phases B and D as given by:

$$L'(\theta) = L_A(\theta) + L_C(\theta) = L_B(\theta) + L_D(\theta) \qquad (8)$$

As shown in Fig. 13, because of the reverse of $L_A(\theta)$ and $L_C(\theta)$, $L'(\theta)$ keeps constant. Thus, according to (4), the reluctance torque is always zero.
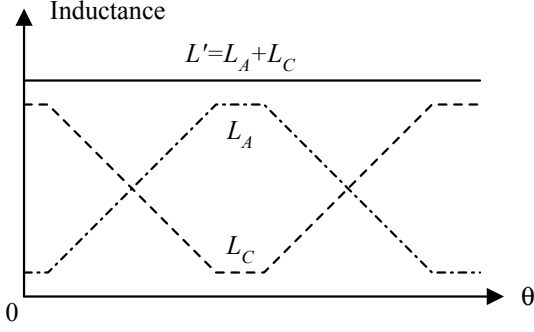
Fig. 13. Theoretical self-inductance.

Moreover, for the DSPM motor with appropriate rotor skewing, the back EMF is very close to sinusoidal waveform as shown in Fig. 14. Assuming that the back EMF of Phase A can be expressed as:

$$e_A = E_m \sin(x) \tag{9}$$

Then the back EMF of Phase B can be obtained by lagging 90° electrical angle as:

$$e_B = E_m \sin(x - 90°) \tag{10}$$

If sinusoidal currents in phase with the back EMFs are properly applied to the phase windings by appropriate control strategy, the PM torque components can be obtained as:

$$T_{pmA} = \frac{e_A i_A}{\omega_r} = \frac{E_m I_m}{\omega_r} \sin^2(x) = T_m \sin^2(x) \tag{11}$$

$$T_{pmB} = \frac{e_B i_B}{\omega_r} = \frac{E_m I_m}{\omega_r} \sin^2(x - 90°) = T_m \sin^2(x - 90°) \tag{12}$$

where $T_m = E_m I_m / \omega_r$ is the magnitude of torque. Then the total electromagnetic torque is:

$$\begin{aligned}
T_e &= T_{pmA} + T_{pmB} = T_m \left[\sin^2(x) + \sin^2(x - 90°) \right] \\
&= T_m \left[\frac{1 - \cos(2x)}{2} + \frac{1 - \cos(2x - 180°)}{2} \right] \\
&= T_m \left[1 - \frac{\cos(2x) + \cos(180° - 2x)}{2} \right] = T_m
\end{aligned} \tag{13}$$

Equation (13) indicates that the total electromagnetic torque does not vary with rotor position and keeps constant, as shown in Fig. 15. This suggests that the doubly salient motor drive is able to compete against the traditional motor drives not only in simple structure, high power density, and fast response etc., but also in the smoothness of torque characteristic.

VI. IMPLEMENTATION AND RESULTS

An experimental split-winding DSPM motor drive with the ratings of 750W and 1500rpm has been designed and built for verification. The main design data are given in Table

II. An IGBT-based four-phase power converter and a micro-computer based digital controller are designed and implemented to drive the motor. A DC dynamometer with the ratings of 2.3kW, 230V and 1500 rpm was used as variable load. Both input power and RMS current of the DSPM motor are measured by a digital power analyzer. Fig. 16 shows a photo of the test set.
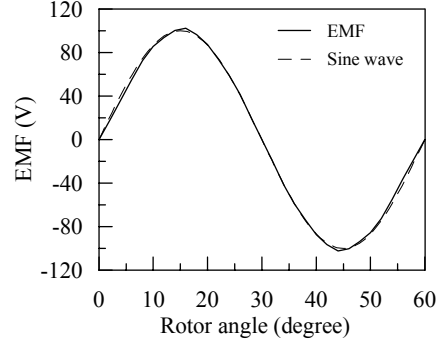

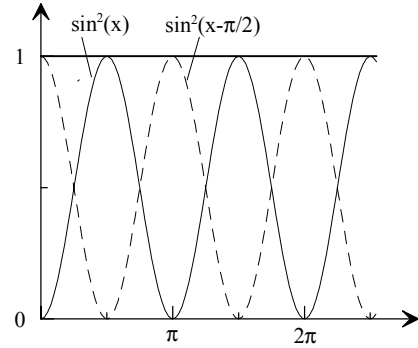Fig. 14. Comparison between back EMF and sine wave.

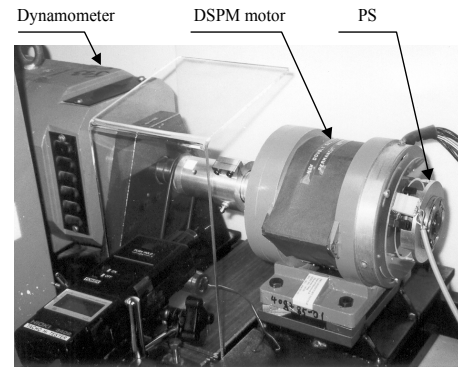Fig. 15. Summation of two torque components.

Fig. 16. Test set of the DSPM motor drive.

Fig. 17 shows the comparison of simulated and measured current waveforms at CCC mode, whereas Fig. 18 shows that at APC mode, illustrating a good agreement between the theoretical and experimental results. Fig. 19 depicts the measured efficiency and RMS current of the motor at the rated speed of 1500 rpm. It is seen that the motor offers high efficiency over wide output power range, which is highly

desirable for some applications such as electric vehicles. The efficiency at the rated operating point is 87.7%, much higher than that of a standard induction motor (typically 75%) with the same capacity and speed.

TABLE II
MOTOR PARAMETERS

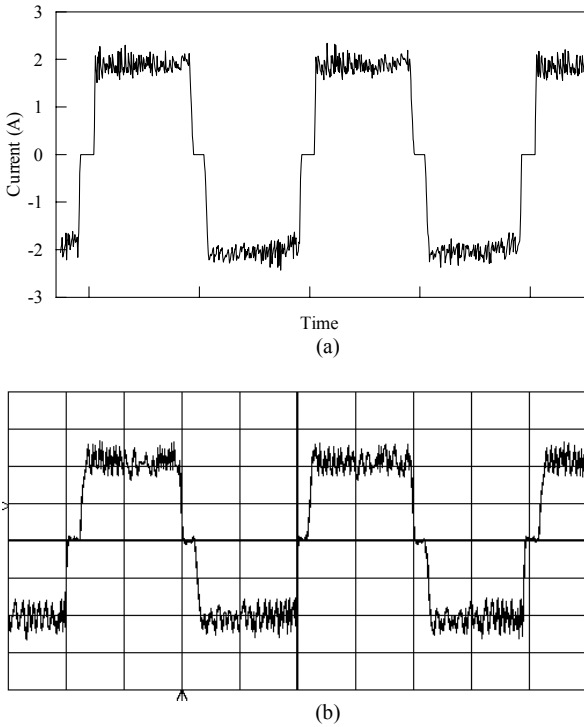|	
Rated power	750 W
Rated phase voltage	200 V
Rated speed	1500 rpm
No. of phases	4
No. of stator poles	8
No. of rotor poles	6
Stator inner diameter	75 mm
Stack length	75 mm
Airgap length	0.45 mm
Winding turns per phase	220
Magnet material	Nd-Fe-B

(a)

(b)

Fig. 17. Current waveforms at CCC mode and 500 rpm. (a) Simulated; (b) measured (1A/div, 5ms/div.

To testify the dynamic performance of the motor drive, the speed and current responses are recorded. Fig. 20(a) shows the starting response from standstill to the rated speed of 1500 rpm. It can be seen that the motor drive responds quickly and takes only 0.43 second to reach the desired speed without steady-state error. Moreover, Fig. 20(b) gives the dynamic performance under a sudden change of load from 2.66 Nm to 0.66 Nm at the rated speed. It can be found that the transient rise in speed is very small and the speed regulation is good.
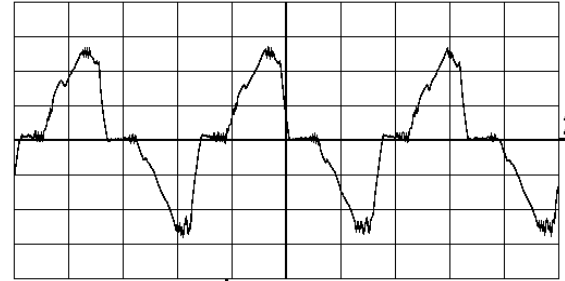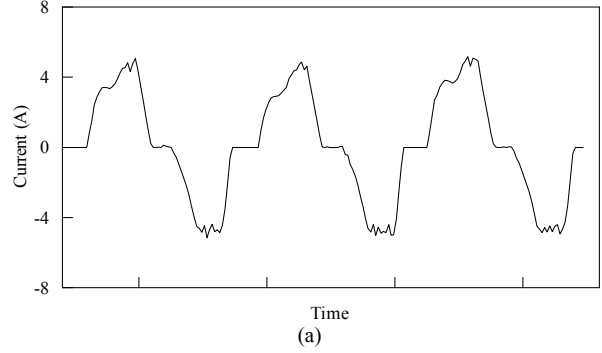

(a)

Fig. 18. Current waveforms at APC mode and 1500 rpm. (a) Simulated, (b) Measured (2A/div, 2ms/div).
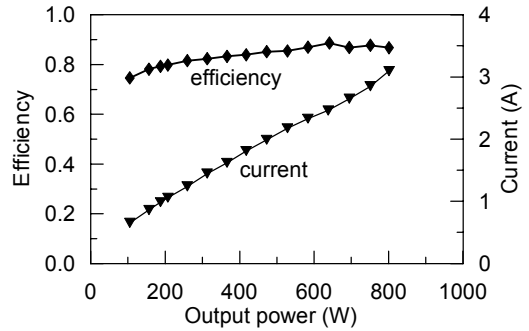

Fig. 19. Measured efficiency and RMS current at 1500 rpm.

Due to the speed limitation of the DC dynamometer available in our laboratory, two alternative tests are carried out in order to testify the effectiveness of the split-winding on extending the constant power operation range of the motor drive. One is the load test under the reduced DC bus voltage from the rated value of 400 V to 150 V. The corresponding measured power-speed characteristics for the winding turns equal to 100% and 50% are shown in Fig. 21. Another is that the DSPM motor is mechanically decoupled with DC dynamometer and runs at no-load. The measured maximum speeds for the winding turns equal to 100% and 50% are 3152 rpm and 6010 rpm, respectively, under the same operation conditions and control parameters. It illustrates that the constant power operation range is almost doubled by reducing the winding turns from 100% to 50%, showing that the split-winding topology can effectively extend the constant power operation range.

The research on the two-phase operation mode of the proposed 8/6-pole DSPM motor drive is under going and the experimental results will be reported in a separate paper in near future.
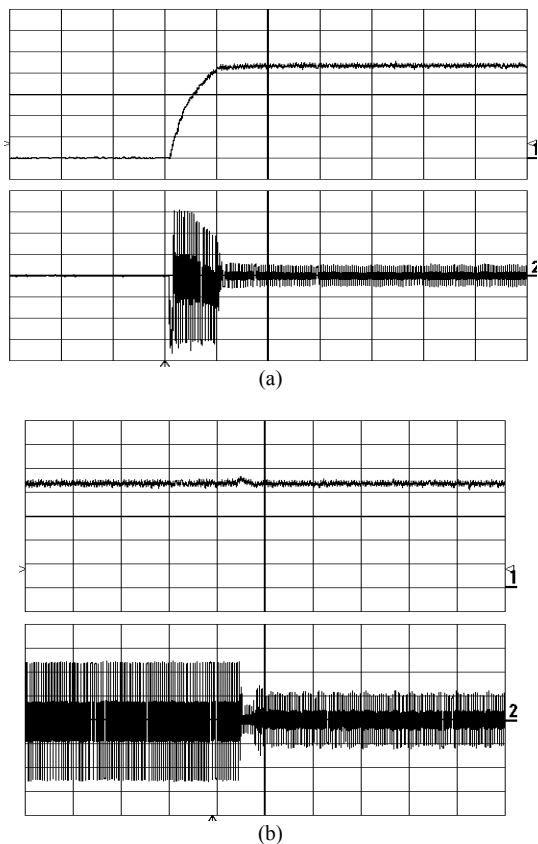

(a)

(b)

Fig. 20. Measured speed (upper trace) and current (lower trace) responses. (a) Starting (350rpm/div, 1.67A/div, 0.5s/div), (b) Sudden change of load from 2.66Nm to 0.66Nm at 1500 rpm (350 rpm/div, 2A/div, 0.5s/div)
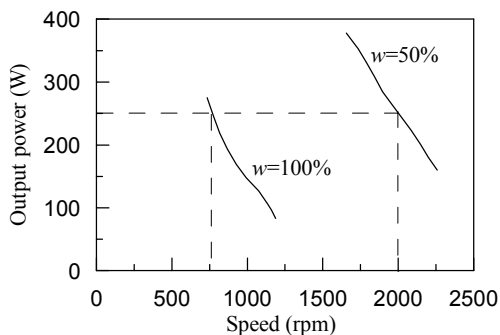

Fig. 21. Measured power-speed characteristics.

VII. CONCLUSIONS

This paper proposes a new 8/6-pole split-winding doubly salient permanent magnet motor drive. The magnetic field distribution of the motor has been analyzed by finite element method. The control strategy of the motor drive has been developed and a digital PI controller combined with bang-

bang control has been specified. A digital control system for the motor drive has been developed based on a 16-bit high-speed microcomputer. According to the unique features of the proposed 8/6-pole DSPM motor, two operation modes, namely four-phase operation and two-phase operation, have been proposed to operate the motor. The analysis of the characteristics of the motor drive has been carried out. A prototype drive system with 4-phase operation mode has been designed, implemented and tested. The results not only verify the theoretical analysis, but also show that the developed control scheme can operate the DSPM motor properly. The proposed 8/6-pole DSPM motor drive offers the advantages of high efficiency over wide power range and good dynamic response. The split-winding topology can effectively extend the constant power operation range. Moreover, the two-phase operation mode of the 8/6-pole DSPM motor offers the potentiality of eliminating the torque ripple of the DSPM motor drive.

REFERENCES

[1] C.C. Chan, J.Z. Jiang, G.H. Chen, X.Y. Wang and K.T. Chau, "A novel polyphase multipole square-wave permanent magnet motor drive for electric vehicles," *IEEE Trans. on Industry Applications*, vol. 30, no. 5, pp. 1258-1265, 1994.

[2] J. Gan, K.T. Chau, C.C Chan and J.Z. Jiang, "A new surface-inset, permanent-magnet, brushless DC motor drive for electric vehicles," *IEEE Trans. on Magnetics*, vol. 36, no. 5, pp. 3810-3818, 2000.

[3] Y. Liao, F. Liang and T.A. Lipo, "A novel permanent magnet motor with doubly salient structure," *IEEE Trans. on Industry Applications*, vol. 31, no. 5, pp. 1059-1078, 1995.

[4] K.T. Chau, Ming Cheng and C.C. Chan, "Performance analysis of 8/6-pole doubly salient permanent magnet motor," *Electric Machines and Power Systems*, vol. 27, no. 10, pp. 1055-1067, 1999.

[5] Ming Cheng, K.T. Chau and C.C. Chan, "Design and analysis of a new doubly salient permanent magnet motor," *IEEE Trans. on Magnetics*, vol. 37, no. 4, pp. 3012-3020, 2001.

[6] Ming Cheng, K.T. Chau, C.C. Chan, E. Zhou and X. Huang, "Nonlinear varying-network magnetic circuit analysis for doubly salient permanent magnet motors," *IEEE Trans on Magnetics*, vol. 36, no. 1, pp. 339-348, 2000.

[7] Ming Cheng and E Zhou, "Analysis and control of novel split-winding doubly salient permanent magnet motor for adjustable speed drive," *Science in China (Series E),* vol. 44, no. 4, pp. 353-364, 2001.

[8] Ming Cheng, E Zhou, X.L. Huang, and Q. Sun, "Split-winding doubly salient permanent magnet machine", Chinese patent ZL 98111107.6, issued on Feb 10, 2001.

[9] K.K. Tan, Q.G. Wang, and C.C. Hang, *Advances in PID Control*, London: Springer, 1999.

[10] F. Blaabjerg, L. Christensen, P.O. Rasmussen, L. Oestergaard, P. Pedersen "New advanced control methods for doubly salient permanent magnet motor," *Record of IEEE Industry Applications Society Annual Meeting*, Orlando, USA, 1995, pp. 272-230.

[11] J. Huang, E. Zhou, and Q. Jiang, "Analysis and compensation of voltage asymmetry in the split converter of a four-phase switched reluctance motor drive," *Proceedings of IEEE International Conference on Power Electronics and Drive Systems*, Singapore, May 1997, pp. 703-707.